nature physics

Article

https://doi.org/10.1038/s41567-024-02543-8

Violation of Bell inequality by photon scattering on a two-level emitter

Received: 21 June 2023

Accepted: 14 May 2024

Published online: 19 June 2024

Check for updates

Shikai Liu[1], Oliver August Dall'Alba Sandberg[1], Ming Lai Chan[1], Björn Schrinski[1], Yiouli Anyfantaki[1], Rasmus B. Nielsen[1], Robert G. Larsen[1], Andrei Skalkin[1], Ying Wang[1], Leonardo Midolo[1], Sven Scholz[2], Andreas D. Wieck[2], Arne Ludwig[2], Anders S. Sørensen[1], Alexey Tiranov[1,3] ✉ & Peter Lodahl[1] ✉

Entanglement, the non-local correlations present in multipartite quantum systems, is a key resource for quantum technologies. It is therefore a major priority to develop simple and energy-efficient methods for generating high-fidelity entangled states. In the case of light, entanglement can be realized by interactions with matter but the required nonlinear interaction is often impractically weak. Here we show how a single two-level emitter deterministically coupled to light in a nanophotonic waveguide can be used to realize photonic quantum entanglement by excitation at the single-photon level. Efficient optical coupling enables mediation of two-photon interactions by the emitter, creating a strong nonlinearity that leads to entanglement. We experimentally verify energy–time entanglement by violating a Bell inequality in an interferometric measurement of the two-photon scattering response. The on-chip two-level emitter acts as a passive scatterer, so that no advanced spin control is required. As such, our method may provide a more efficient approach to synthesizing photonic entangled states for quantum simulators or metrology.

The interaction between a quantum pulse of light and a two-level emitter (Fig. 1a,d) constitutes a new experimental paradigm in quantum optics[1,2]. Despite its conceptual simplicity, substantial quantum complexity can be encoded in the system since a quantum pulse represents an infinitely large (continuous) Hilbert space. Moreover, a two-level emitter can implement a highly nonlinear operation on the incoming pulse without the need for demanding and error-susceptible emitter preparation schemes. To enhance the photon–photon nonlinearity, the main experimental challenge is to promote the radiative coupling of the emitter, ensuring its dominance over deteriorating decoherence processes. Considerable advancements have been made in the past decades using semiconductor quantum dots (QDs) in photonic crystal waveguides (PhC WGs) and cavities[3] (see the illustration of a PhC WG device in Fig. 1d).

The quantum nonlinear response is the subject of an ongoing research effort, using a variety of emitters, including QDs[4], colour centres in diamonds[5], atoms[6] and molecules[7]. Experimental advancements include the observation of antibunching[8], quadrature squeezing of light in resonance fluorescence[9,10], and two-photon correlation dynamics and photonic bound states[11–13]. Extending to multiple emitters and/or including spin degrees of freedom will facilitate photon sorters for deterministic Bell state analysers[14], quantum logic gates[15,16] and single-photon transistors[17]. Furthermore, many-body waveguide quantum electrodynamics may be pushed to new realms of strongly correlated light and matter[18,19]. It was theoretically predicted that the two-level nonlinear response can induce photon–photon correlations[1]; however, it has not been explored whether this nonlinearity enables the realization of non-local quantum entanglement.

[1]Center for Hybrid Quantum Networks, The Niels Bohr Institute, University of Copenhagen, Copenhagen, Denmark. [2]Lehrstuhl für Angewandte Festkörperphysik, Ruhr-Universität Bochum, Bochum, Germany. [3]Present address: Institut de Recherche de Chimie Paris, Chimie ParisTech, Université PSL, CNRS, Paris, France. ✉e-mail: alexey.tiranov@chimieparistech.psl.eu; lodahl@nbi.ku.dk

https://doi.org/10.1038/s41567-024-02543-8

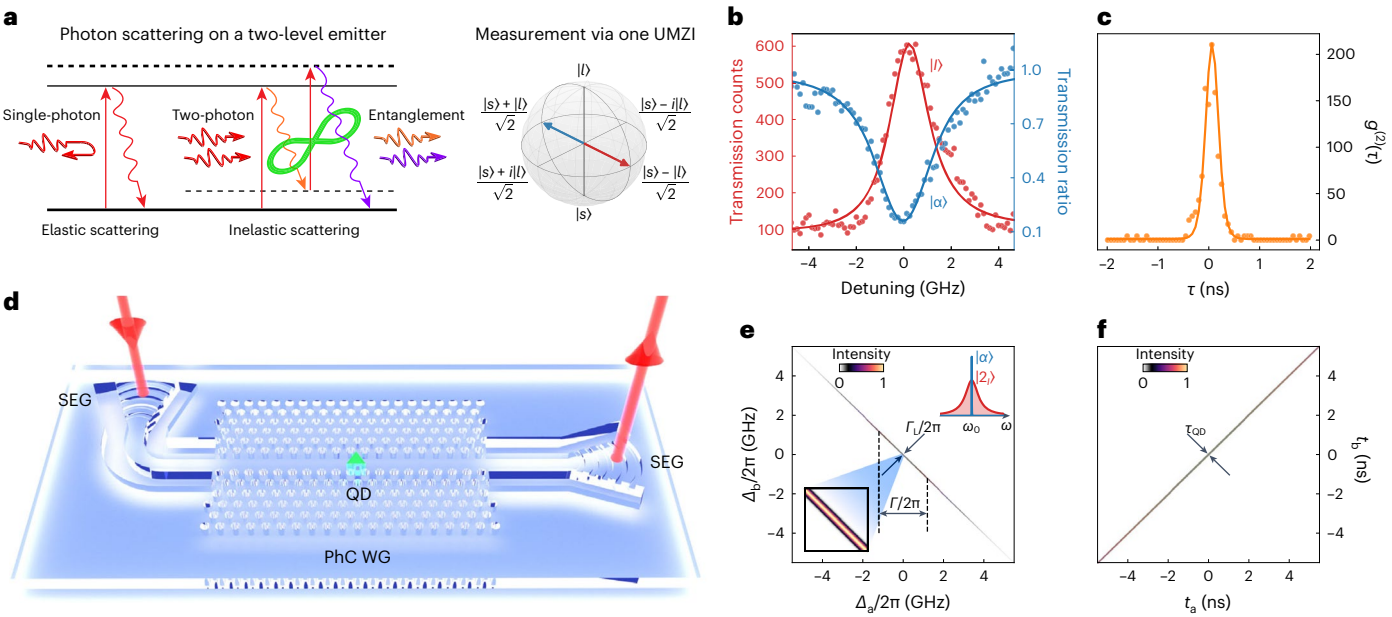

Fig. 1 | Two-photon energy–time entanglement induced by coherent interaction of two photons with a QD integrated into a PhC WG. a, The operational principle of the photon scattering and entanglement processes. A single-photon wave packet is predominantly reflected by elastic scattering on a two-level emitter, while the two-photon wave packet can be inelastically scattered in the forward direction, thereby generating energy–time entanglement. The entanglement is probed using two UMZIs (Fig. 2). Each UMZI is used to realize time projections onto the superposition state $\frac{|s\rangle+e^{i\phi}|l\rangle}{\sqrt{2}}$, as illustrated on a Bloch sphere, where $|s\rangle$ ($|l\rangle$) corresponds to a photon taking the short (long) path, and ϕ is the phase setting of the UMZI. $\phi = 0$ (blue vector) and $\phi = \pi$ (red vector) refer to the two settings for data in **b**. **b**, Transmission intensity measurements through the PhC WG and one UMZI versus QD detuning. The blue curve indicates the transmission dip by resonant scattering of a weak coherent state $|\alpha\rangle$. Suppression of the elastically scattered laser photons by a destructive interference phase ($\phi = \pi$) reveals inelastically scattered photons $|l\rangle$ (red). **c**, The measured normalized second-order correlation function $g^{(2)}(\tau)$ of the light transmitted through the PhC WG on resonance with the QD, reaching values above 200. **d**, A schematic of the QD-embedded PhC WG structure with two mode adaptors, including shallow-etched gratings (SEGs) and nanobeam waveguides. **e**, The calculated normalized joint spectral intensity for laser linewidth $\Gamma_L/2\pi = 100$ kHz, a Purcell enhanced QD linewidth of $\Gamma/2\pi = 2.3$ GHz, assuming ideal coupling of QD to the PhC WG. $\Delta_{a(b)} = \omega_{a(b)} - \omega_L$ is the frequency difference between output photon ($\omega_{a(b)}$) and the input laser (ω_L). The width of the biphoton spectrum is determined by the laser linewidth Γ_L, while each photon is broadened by the QD linewidth Γ. Top right insert: spectra of the input coherent state $|\alpha\rangle$ (blue) and the output biphoton state $|2_l\rangle$ (red). Bottom left insert: enlarged joint spectral intensity spanning a range of 1 MHz. **f**, The corresponding normalized joint temporal intensity. The biphoton correlation time is determined by the QD lifetime τ_{QD} (see Supplementary Note 6 for characterization).

In this Article, we demonstrate experimentally that a two-level quantum emitter radiatively coupled to a PhC WG can induce strong energy–time entanglement between two scattered photons (Fig. 1a). The correlations are found to violate a Bell inequality and, therefore, local realism under the fair-sampling assumption. The experiment couples a continuous wave (incoming light) with a discrete quantum system (emitter), offering a pathway to non-Gaussian photonic operations that are highly sought after in continuous-variable quantum computing architectures[20]. Previous research towards entanglement generation with quantum emitters exploited the strong excitation (Mollow) regime in bulk samples[21] or the QD biexciton radiative cascade[22,23]. In contrast, our scheme relies on passive scattering of a weak excitation field by a two-level QD in a PhC WG to induce genuine entanglement. This work introduces a conceptually different and advantageous approach to energy–time entanglement generation that may serve as an attractive alternative to four-wave mixing sources[24], since it operates at the ultralow energy consumption level of single photons and does not require complex and decoherence-sensitive pumping schemes.

We consider a single two-level emitter deterministically coupled to a single propagating spatial mode in a PhC WG (Fig. 1d). A weak coherent input field is launched into the PhC WG and interacts with the emitter of coupling efficiency $\beta = \gamma/\Gamma$, governed by the ratio between the radiative decay rate into the waveguide mode γ and the QD total decay rate Γ (ref. 25). For $\beta = 1$ with no decoherence processes, the single-photon component is elastically reflected via interaction with the emitter, while the two-photon component can be inelastically scattered into the forward (transmission) direction, as shown in Fig. 1a. The latter process can be interpreted as an emitter 'dressing' where two virtual energy levels (dashed lines) act as intermediaries for the energy exchange between two photons during their inelastic collisions. The energy exchanged between the photons is governed by the emitter linewidth, while the total energy of the two photons is fixed by energy conservation. An alternative interpretation is formulated in the time domain: one photon excites the emitter and the second photon stimulates the emission, causing accelerated decay and photon bunching in the forward direction. Since the two outgoing photons are correlated in both energy and time, they become entangled by the interaction. Experimentally, the two-photon scattering process is studied in a Franson interferometer[26] with time-resolved photon correlation measurements under the regime of weak resonant excitation, that is, far below the saturation threshold of the emitter (Fig. 2). In this way, a Clauser–Horn–Shimony–Holt (CHSH) Bell inequality entanglement criterion can be tested where a Bell parameter of $S = 2$ constitutes the locality bound[27]. Various experimental imperfections influence S, including the finite photon-emitter coupling efficiency (β factor), pure dephasing rate (γ_d relative to the emitter linewidth Γ) and the strength of the incoming light (mean photon number within the emitter lifetime n). These imperfections result in a single-photon component (elastic scattering) that is not fully reflected, thereby reducing S. We find that S is sensitive to γ_d, Γ and n to first-order but is remarkably robust to coupling loss, with a quartic dependence in the limit of $\beta \to 1$:

$$S(\beta) \approx 2\sqrt{2}\left[1-(1-\beta)^4\right]. \quad (1)$$

https://doi.org/10.1038/s41567-024-02543-8

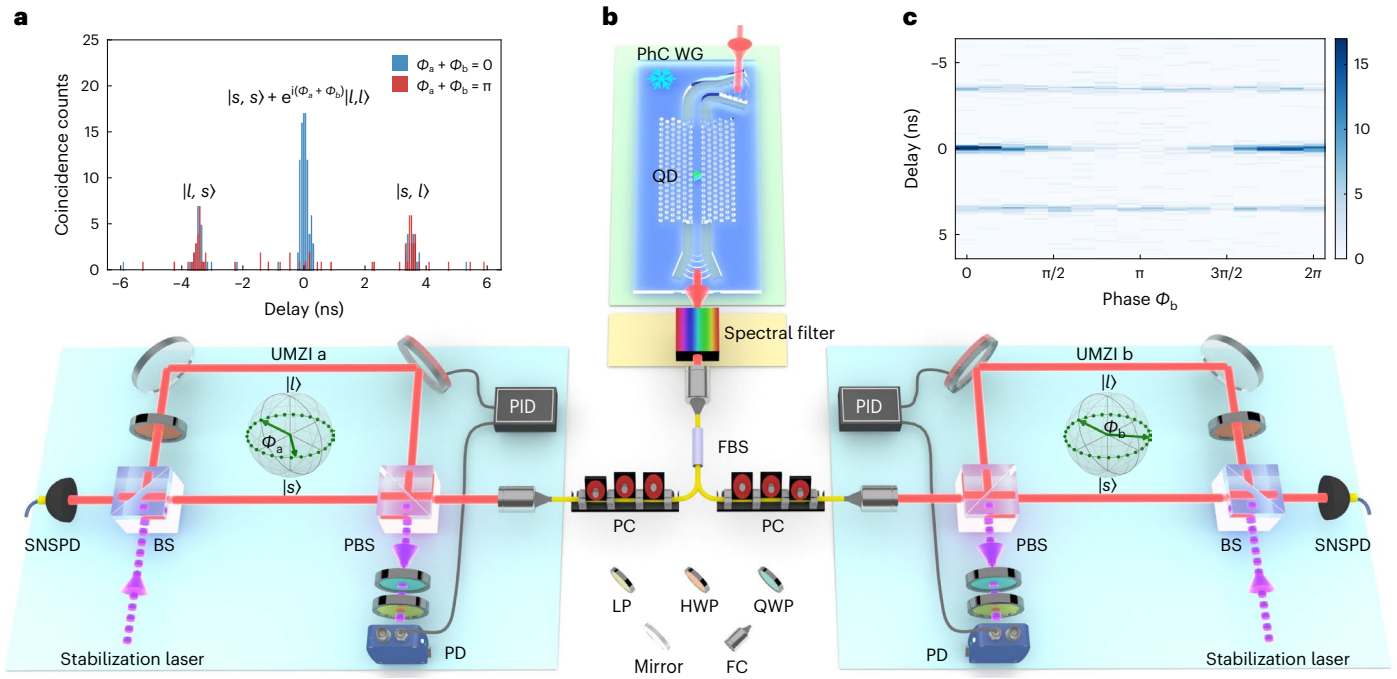

Fig. 2 | Experimental setup and characterization of two-photon energy–time entanglement. a, Time correlation histograms of coincidence counts for constructive (blue, $\phi_a + \phi_b = 0$) and destructive (red, $\phi_a + \phi_b = \pi$) interference between two photons traversing the short (s) and long (l) paths of the UMZIs, respectively. **b**, Experimental setup including the PhC WG chip (light-green area), spectral filter (light-orange area) and the Franson interferometer (light-blue areas). The two Bloch spheres illustrate the two independently controlled phases ϕ_a and ϕ_b. SNSPD, superconducting nanowire single-photon detector; FC, fibre collimator; PC, polarization controller; FBS, fibre beam splitter; PD, photodiode; PID, proportional–integral–derivative. To control the phase difference between the two interferometer paths, we actively stabilize the UMZIs with a PID module locked by the same laser that excites the QD. **c**, Two-dimensional correlation histogram of coincidence counts versus phase and time delay.

The complete theory is presented in Supplementary Note 8, where the experimental requirements for violating the Bell inequality are also benchmarked in detail (Supplementary Fig. 7).

The quantum correlations induced by the nonlinear scattering are illustrated by the two-photon joint spectral and temporal intensity distributions in Fig. 1e,f. The input weak coherent state $|\alpha\rangle$ resembles a Dirac delta function in frequency, while the output entangled photon pair $|2_l\rangle$ is Lorentzian broadened by the QD linewidth Γ. It can be expressed as $|2_l\rangle = \frac{1}{2}\int \mathrm{d}\Delta \mathcal{T}_{\Delta,-\Delta}\,|1_\Delta\rangle\,|1_{-\Delta}\rangle$ (Supplementary Note 7), where $\Delta = \Delta_a = -\Delta_b$ is the frequency detuning of each outgoing photon relative to the pump frequency, and $\mathcal{T}_{\Delta,-\Delta} = -4\beta^2/[\pi\Gamma(1 + 4\frac{\Delta^2}{\Gamma^2})]$ is the two-photon Lorentzian spectrum[28]. Energy conservation demands $2\omega_L = \omega_a + \omega_b$, which introduces anti-correlation in the two-photon joint spectral density (Fig. 1e). The time uncertainty of the generated photon pair is determined by the pump laser coherence time $\tau_L > 1\,\mu s$ (inversely proportional to the laser linewidth $\Gamma_L/2\pi \approx 100$ kHz), which is much longer than the Purcell enhanced QD lifetime $\tau_{QD} \approx 69$ ps (Fig. 1f).

Figure 1b measures the transmission intensity of scattered photons versus the QD detuning after an unbalanced Mach–Zehnder interferometer (UMZI) at two different phases ϕ (see the UMZI setup in Fig. 2b). This allows separate measurements of either the extinction of a weak coherent state (blue, $\phi = 0$) or the inelastically scattered photons (red, $\phi = \pi$). During resonant scattering, the single-photon component is primarily reflected due to destructive interference in the PhC WG, while the transmitted light consists of residual coherent photons from the laser and inelastically scattered photons. Upon entering the UMZI, the laser photons interfere with themselves at a beam splitter (BS) dependent on the interferometer phase ϕ, whereas the inelastic photons, scattered off the QD, do not (see Supplementary Note 5 for UMZI design details). For $\phi = 0$, elastic scattering dominates as the laser photons traversing the short and long paths constructively interfere, thereby revealing a transmission dip (Fig. 1b, blue data). Conversely, for $\phi = \pi$, the laser photons destructively interfere, allowing direct observation of the inelastically scattered photons (Fig. 1b, red data).

The pronounced extinction of the transmission intensity (beyond 85%) is indicative of the efficient radiative coupling to the PhC WG and is representative of the performance of QD PhC WG devices[28]. By modelling the experimental data sets, we extract $\beta \approx 92\%$ and a Purcell enhancement from slow light in the PhC WG of $F_P \approx 15.9$, which increases the QD decay rate to $\Gamma/2\pi = 2.3$ GHz (compared with ~0.14 GHz for QDs in bulk[29]). In the entanglement characterization discussed below, a narrow bandwidth notch filter is implemented to suppress residual laser leakage due to a non-unity β factor and minor residual slow spectral diffusion (see Supplementary Note 2 and Supplementary Fig. 8 for further details).

The successful preparation of a two-photon component is quantified by second-order photon correlation measurements. In a recent study of atomic resonance fluorescence, the photon statistics were found to transition from antibunching to bunching by spectral filtering[13]. Our QD-WG device exhibits bunching statistics in resonance transmission even without filtering, but the bunching is further enhanced by applying a similar filter (see Supplementary Note 2 for details). We observe a pronounced photon bunching of $g^{(2)}(0) \approx 210$ (Fig. 1c), which explicitly demonstrates that the incoming Poissonian photon distribution is substantially altered by the strong nonlinear interaction with the QD[28]. The theoretical model does not explicitly include the filter yet accurately describes the experimental data of Fig. 1c, by adjusting the input model parameters (see Supplementary Notes 4 and 8e for the full details on data modelling).

Figure 2b illustrates the experimental setup. The scattered light from the QD PhC WG is spectrally filtered and directed by a non-polarizing fibre BS to two identical UMZIs for entanglement analysis. The time difference between the two paths of each UMZI is set to $\tau_I = 3.6$ ns, which is shorter than τ_L and longer than the two-photon

https://doi.org/10.1038/s41567-024-02543-8

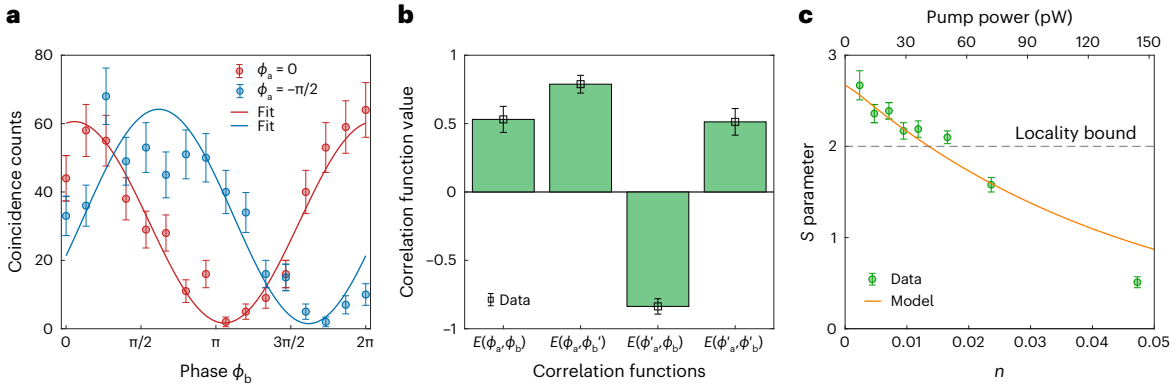

Fig. 3 | Two-photon Franson interference measurements and observation of a violation of the CHSH inequality. a, Interference curves as a function of ϕ_b with ϕ_a fixed at 0 (red) and −π/2 (blue). The data are fitted to a sinusoidal model from which a visibility of 95(4)% is extracted. **b**, Measured correlation functions from which $S = 2.67(16)$ is recorded. **c**, S parameter versus n (bottom x axis) or the corresponding pump power in the PhC WG (top x axis). n and pump powers are calibrated by fitting the full set of transmission intensity data (Supplementary Note 3). The solid curve is the theoretical model (Supplementary Note 8e) with parameters taken from the filtered power saturation $g^{(2)}$ measurements in Supplementary Note 4, that is, no additional fitting was performed. The dashed black line represents the locality bound. The data in **a** and **b** are recorded for the lowest n (0.0024) or pump power (7.2 pW) in **c**. As we have performed single-shot measurements, the error bars shown are standard deviations obtained from Monte Carlo simulations with 1,000 samples, assuming a Poisson distribution with a mean given by the measured value (shown as markers).

correlation time set by τ_{QD}. We implement two-photon Franson interference measurements by recording time-resolved correlations between photon pairs while controlling the interferometric phases (ϕ_a and ϕ_b). Figure 2a reveals three distinct correlation peaks, corresponding to every possible path that the two photons can take separately: long–short $|l,s\rangle$ (left peak), short–short $|s,s\rangle$ or long–long $|l,l\rangle$ (central peak), and short–long $|s,l\rangle$ (right peak). For the central peak, the two paths $|s,s\rangle$ and $|l,l\rangle$ cannot be distinguished, due to the long coherence time of the pump laser shared by the entangled pair ($\tau_L \gg \tau_I$) and the erased which-path information. Effectively, the UMZIs project the two-photon energy–time entangled state into two discrete time bins (early and late) separated by τ_I, When two photons scatter off the emitter in the same time bin, the first photon saturates the emitter, whereas the second can be transmitted by stimulated emission, causing two-photon bunching in the forward direction. This process induces time and energy correlation between the two photons. Using two UMZIs, photons in the early time bin taking the long paths will interfere with photons in the late time bin taking the short paths. This equivalently projects the state onto the path entangled state $|s,s\rangle + e^{i(\phi_a+\phi_b)}|l,l\rangle$. By tuning UMZIs' phases such that $\phi_a + \phi_b = 0(\pi)$, we observe constructive (destructive) interference of the central peak (Fig. 2a), stemming from the two-photon energy–time entanglement. By further measuring a two-dimensional histogram shown in Fig. 2c, almost background-free quantum interference is observed as a testimony of the highly efficient spectral selection of the two-photon scattering component (see Supplementary Note 5 for background noise comparison between filtered and unfiltered data).

In Fig. 3a, we scan the phase ϕ_b for two different phase settings of interferometer a ($\phi_a = 0, -\pi/2$). The Franson interference visibility is defined as $V = (R_{max} - R_{min})/(R_{max} + R_{min})$, where R_{min} (R_{max}) is the coincidence rate of the central peak at the minimum (maximum) of the interference curve. To obtain higher count rates with smaller fluctuations (error bars), the coincidence time window is increased to 0.512 ns compared with its counterpart (0.064 ns) in Figs. 1 and 2. Fitting the data with a sinusoid, we extract an interference visibility of $V = 95(4)\%$, which indicates the presence of entanglement[30].

The energy–time entangled photon pair induced by the nonlinear interaction is thoroughly certified with a CHSH Bell inequality test[27]. The CHSH S parameter is defined as $S = |E(\phi_a, \phi_b) + E(\phi_a, \phi_{b'}) - E(\phi_{a'}, \phi_b) + E(\phi_{a'}, \phi_{b'})|$, where $E(\phi_a, \phi_b)$ denotes the correlation function required for the CHSH inequality, which is a combination of four unnormalized $g^{(2)}$ after the UMZIs at different phase settings (Supplementary Note 8d). Figure 3b shows the strongest correlations measured at the lowest value of n in Fig. 3c, which corresponds to a pump power of 7.2 pW at a single-photon level. We record a pronounced violation of the CHSH Bell inequality $S = 2.67(16) > 2$ by more than four standard deviations. This validates that non-local quantum correlations can be induced by two-photon inelastic scattering off a deterministically coupled two-level emitter. Figure 3c explores the power dependence of the S parameter, and the experimental data agree well with the theoretical model detailed in Supplementary Note 8e. The entanglement quality is primarily limited by photon distinguishability contributions from pure dephasing, as well as multi-photon scattering processes from finite n.

We have experimentally demonstrated the violation of the CHSH Bell inequality by weak scattering of a single two-level emitter deterministically coupled to light in a PhC WG. While spin-based systems can be more versatile in generating entangled states, our passive scattering approach offers ease of operation, as it requires no elaborate excitation or active spin control, and spin decoherence processes do not play a role. This could reduce the appreciable overhead for future up-scaling of entanglement generation schemes. Compared to traditional χ^2 and χ^3 nonlinear parametric processes that require strong pump fields, our approach exploits a saturable two-level emitter operating at the single-photon level, resulting in a much higher power efficiency. The single-photon nonlinearity is enabled by waveguide interference, which ideally reflects single photons and transmits photon-bound states responsible for time–energy entanglement[1]. This allows the realization of an entanglement source with a spectral brightness far beyond the capabilities of most parametric sources (see Supplementary Note 9 for further comparison), and the approach offers a route to non-Gaussian photonic quantum operations[31,32]. These unique attributes hold a promising alternative for efficiently generating on-chip energy–time entangled photons with high fidelity. Future experiments could exploit the creation of high-dimensional entanglement[33] and the synthesis of photonic quantum states useful for quantum optics neural network[34]. Another promising direction is to engineer the inelastic scattering processes by many-body subradiant states using coupled QDs[35,36]. Waveguide-mediated quantum nonlinear interactions will prove essential to applications within photonic quantum computing[37], quantum communication[38] and quantum sensing[39,40].

Online content

Any methods, additional references, Nature Portfolio reporting summaries, source data, extended data, supplementary information, acknowledgements, peer review information; details of author contributions and competing interests; and statements of data and code availability are available at https://doi.org/10.1038/s41567-024-02543-8.

References

1. Shen, J.-T. & Fan, S. Strongly correlated two-photon transport in a one-dimensional waveguide coupled to a two-level system. *Phys. Rev. Lett.* **98**, 153003 (2007).
2. Kiilerich, A. H. & Mølmer, K. Input-output theory with quantum pulses. *Phys. Rev. Lett.* **123**, 123604 (2019).
3. Lodahl, P., Ludwig, A. & Warburton, R. J. A deterministic source of single photons. *Phys. Today* **75**, 44–50 (2022).
4. Javadi, A. et al. Single-photon non-linear optics with a quantum dot in a waveguide. *Nat. Commun.* **6**, 8655 (2015).
5. Sipahigil, A. et al. An integrated diamond nanophotonics platform for quantum-optical networks. *Science* **354**, 847–850 (2016).
6. Hamsen, C., Tolazzi, K. N., Wilk, T. & Rempe, G. Two-photon blockade in an atom-driven cavity qed system. *Phys. Rev. Lett.* **118**, 133604 (2017).
7. Pscherer, A. et al. Single-molecule vacuum rabi splitting: four-wave mixing and optical switching at the single-photon level. *Phys. Rev. Lett.* **127**, 133603 (2021).
8. Hanschke, L. et al. Origin of antibunching in resonance fluorescence. *Phys. Rev. Lett.* **125**, 170402 (2020).
9. Schulte, C. H. H., Hansom, J., Jones, A. E., Matthiesen, C., Le Gall, C. & Atatüre, M. Quadrature squeezed photons from a two-level system. *Nature* **525**, 222–225 (2015).
10. Hinney, J. et al. Unraveling two-photon entanglement via the squeezing spectrum of light traveling through nanofiber-coupled atoms. *Phys. Rev. Lett.* **127**, 123602 (2021).
11. Jeannic, H. L. et al. Dynamical photon–photon interaction mediated by a quantum emitter. *Nat. Phys.* **18**, 1191–1195 (2022).
12. Tomm, N. et al. Photon bound state dynamics from a single artificial atom. *Nat. Phys.* **19**, 857–862 (2023).
13. Masters, L. et al. On the simultaneous scattering of two photons by a single two-level atom. *Nat. Photon.* **17**, 972–976 (2023).
14. Witthaut, D., Lukin, M. D. & Sørensen, A. S. Photon sorters and qnd detectors using single photon emitters. *Europhys. Lett.* **97**, 50007 (2012).
15. Konyk, W. & Gea-Banacloche, J. Passive, deterministic photonic conditional-phase gate via two-level systems. *Phys. Rev. A* **99**, 010301 (2019).
16. Krastanov, S., Jacobs, K., Gilbert, G., Englund, D. R. & Heuck, M. Controlled-phase gate by dynamic coupling of photons to a two-level emitter. *npj Quantum Inf.* **8**, 103 (2022).
17. Chang, D. E., Sørensen, A. S., Demler, E. A. & Lukin, M. D. A single-photon transistor using nanoscale surface plasmons. *Nat. Phys.* **3**, 807–812 (2007).
18. Fayard, N., Henriet, L., Asenjo-Garcia, A. & Chang, D. E. Many-body localization in waveguide quantum electrodynamics. *Phys. Rev. Res.* **3**, 033233 (2021).
19. Bello, M., Platero, G. & González-Tudela, A. Spin many-body phases in standard- and topological-waveguide qed simulators. *PRX Quantum* **3**, 010336 (2022).
20. Bourassa, J. E. et al. Blueprint for a scalable photonic fault-tolerant quantum computer. *Quantum* **5**, 392 (2021).
21. Peiris, M., Konthasinghe, K. & Muller, A. Franson interference generated by a two-level system. *Phys. Rev. Lett.* **118**, 030501 (2017).
22. Jayakumar, H. et al. Deterministic photon pairs and coherent optical control of a single quantum dot. *Phys. Rev. Lett.* **110**, 135505 (2013).
23. Hohn, M. et al. Energy–time entanglement from a resonantly driven quantum-dot three-level system. *Phys. Rev. Res.* **5**, L022060 (2023).
24. Glorieux, Q. et al. Double-Λ microscopic model for entangled light generation by four-wave mixing. *Phys. Rev. A* **82**, 033819 (2010).
25. Lodahl, P., Mahmoodian, S. & Stobbe, S. Interfacing single photons and single quantum dots with photonic nanostructures. *Rev. Mod. Phys.* **87**, 347 (2015).
26. Franson, J. D. Bell inequality for position and time. *Phys. Rev. Lett.* **62**, 2205 (1989).
27. Clauser, J. F., Horne, M. A., Shimony, A. & Holt, R. A. Proposed experiment to test local hidden-variable theories. *Phys. Rev. Lett.* **23**, 880 (1969).
28. Le Jeannic, H. et al. Experimental reconstruction of the few-photon nonlinear scattering matrix from a single quantum dot in a nanophotonic waveguide. *Phys. Rev. Lett.* **126**, 023603 (2021).
29. Arcari, M. et al. Near-unity coupling efficiency of a quantum emitter to a photonic crystal waveguide. *Phys. Rev. Lett.* **113**, 093603 (2014).
30. Kwiat, P. G., Steinberg, A. M. & Chiao, R. Y. High-visibility interference in a Bell-inequality experiment for energy and time. *Phys. Rev. A* **47**, R2472 (1993).
31. Walschaers, M. Non-gaussian quantum states and where to find them. *PRX Quantum* **2**, 030204 (2021).
32. Andersen, U. L., Neergaard-Nielsen, J. S., van Loock, P. & Furusawa, A. Hybrid discrete- and continuous-variable quantum information. *Nat. Phys.* **11**, 713–719 (2015).
33. Martin, A. et al. Quantifying photonic high-dimensional entanglement. *Phys. Rev. Lett.* **118**, 110501 (2017).
34. Steinbrecher, G. R., Olson, J. P., Englund, D. & Carolan, J. Quantum optical neural networks. *npj Quantum Inf.* **5**, 60 (2019).
35. Ke, Y., Poshakinskiy, A. V., Lee, C., Kivshar, Y. S. & Poddubny, A. N. Inelastic scattering of photon pairs in qubit arrays with subradiant states. *Phys. Rev. Lett.* **123**, 253601 (2019).
36. Tiranov, A. et al. Collective super- and subradiant dynamics between distant optical quantum emitters. *Science* **379**, 389–393 (2023).
37. Alexander, R. N. et al. One-way quantum computing with arbitrarily large time-frequency continuous-variable cluster states from a single optical parametric oscillator. *Phys. Rev. A* **94**, 032327 (2016).
38. Zhong, T. et al. Photon-efficient quantum key distribution using time–energy entanglement with high-dimensional encoding. *N. J. Phys.* **17**, 022002 (2015).
39. Sánchez Muñoz, C., Frascella, G. & Schlawin, F. Quantum metrology of two-photon absorption. *Phys. Rev. Res.* **3**, 033250 (2021).
40. Kaiser, F. et al. Quantum enhancement of accuracy and precision in optical interferometry. *Light.: Sci. Appl.* **7**, 17163 (2018).

Methods

Sample information

The used PhC WG device is fabricated on a suspended GaAs membrane of thickness 180 nm, forming a *p*–i–*n* diode heterostructure where InAs QDs are embedded. Two mode adaptors are designed to guide light in and out of the PhC WG, with the sample mounted in a cryostat operating at 4 K. More details can be found in Supplementary Note 1.

Phase locking of UMZIs

In Fig. 2b, the beam from another laser is introduced in each UMZI for phase stabilization. The stabilization beam with horizontal polarization is split into two paths by the BS and then recombined at the polarizing beam splitter (PBS) with linear cross-polarization due to the half-wave plate (HWP) at 45° in the long path. After the quarter-wave plate (QWP) at 45°, the stabilization beam becomes circularly cross-polarized and then interferes with itself at the linear polarizer (LP). The interferometric phase can be projected to the entangled beam and tuned by rotating the angle of the LP. Meanwhile, a photodiode, a piezo-mounted mirror and a PID module constitute the real-time negative feedback loop, which allows each UMZI to be locked stably and long enough for data acquisition.

Data availability

Source data are provided with this paper. Other data that support the findings of this study are available from the corresponding authors upon reasonable request.

Code availability

The code used for data analysis and simulated results is available from the corresponding authors upon reasonable request.

Acknowledgements

We gratefully acknowledge financial support from Danmarks Grundforskningsfond (DNRF 139, Hy-Q Center for Hybrid Quantum Networks), the Novo Nordisk Foundation (Challenge project 'Solid-Q'). Furthermore, this project has received funding from the European Union's Horizon 2020 research and innovation programmes under grant agreement no. 824140 (TOCHA, H2020-FETPROACT-01-2018). B.S. acknowledges financial support from Deutsche Forschungsgemeinschaft (DFG, German Research Foundation), grant no. 449674892. O.A.D.S. acknowledges funding from the European Union's Horizon 2020 research and innovation programme under the Marie Skłodowska-Curie grant agreement no. 801199. M.L.C. acknowledges funding from the European Union's Horizon 2020 Research and Innovation programme under grant agreement no. 861097 (project name QUDOT-TECH).

Author contributions

S.L. and A.T. performed the experiments based on interferometers built by R.B.N., R.G.L. and Y.A. S.L. and A.T. carried out the measurements, and analysed the data with help from M.L.C. and A.S. S.L. prepared the figures with input from A.T., A.S.S. and P.L. O.A.D.S. developed the theory with input from B.S. and A.S.S. S.L., A.T., O.A.D.S. and P.L. wrote the manuscript with input from all the authors. S.S., A.D.W. and A.L. prepared the wafer. Y.W. and L.M. fabricated the chip. A.T. and P.L. conceived the idea and supervised the project.

Competing interests

P.L. is the founder of the company Sparrow Quantum, which commercializes single-photon sources. The other authors declare no competing interests.

Additional information

Supplementary information The online version contains supplementary material available at https://doi.org/10.1038/s41567-024-02543-8.

Correspondence and requests for materials should be addressed to Alexey Tiranov or Peter Lodahl.

Peer review information *Nature Physics* thanks the anonymous reviewers for their contribution to the peer review of this work.